Zhang X *et al.* (2023)
Notulae Botanicae Horti Agrobotanici Cluj-Napoca
Volume 51, Issue 3, Article number 13150
DOI:10.15835/nbha51313150
Research Article

Metabolome and transcriptome analyses reveal the colouring mechanism of red honeysuckle (*Lonicera japonica* Thunb.)

Xiaodong ZHANG[1a*], Caixia LI[2b*], Zhanchao HAO[3]

[1]*Xuchang University, Food and Pharmacy College, 88 Bayi Road, Xuchang 461000, Henan, China; zxd95@xcu.edu.cn (*corresponding author)*
[2]*Xuchang University, Key Laboratory of Micro-Nano Materials for Energy Storage and Conversion of Henan Province, Institute of Surface Micro and Nano Materials, College of Chemical and Materials Engineering, 88 Bayi Road, Xuchang 461000, Henan, China; 20201009@xcu.edu.cn (*corresponding author)*
[3]*Yuzhou Traditional Chinese Medicine Standardization Center, Yuzhou 461670, Henan, China; yzszyb666@126.com*
[a,b] *These authors contributed equally to the work*

Abstract

Honeysuckle has been widely used as a medicinal herb and food additive in China for a long time. However, little is known about the pigment composition and colouring mechanism of red honeysuckle, which is a rare germplasm resource. This study aims to investigate the anthocyanin components and colouring mechanism of red honeysuckle, and to identify potential regulatory genes in the anthocyanin biosynthesis pathway. 'Yujin 1' and 'Yujin 2', with yellow-white and red flower buds, respectively, were selected for the study. Using a metabolomics method, we identified the anthocyanin components, while transcriptomics analysis was used to mine the structural and regulatory genes of the anthocyanin biosynthesis pathway. Additionally, protein-protein interaction analysis was employed to predict the regulation mechanism of anthocyanin biosynthesis. The results revealed that cyanidin-3,5-O-diglucoside, peonidin-3,5-O-diglucoside, and cyanidin-3-O-glucoside were the main pigment components of red honeysuckle. We also constructed a possible anthocyanin biosynthetic pathway and identified MYB and bHLH transcription factors that may play regulatory roles in this pathway. Furthermore, our findings suggest that bHLH23 may regulate anthocyanin biosynthesis by binding to the *DFR* gene promoter. These findings have significant implications for breeding new honeysuckle varieties and developing functional foods and medicines.

Keywords: anthocyanin; colouring mechanism; *Lonicera japonica*; metabolome; transcriptome

Introduction

Lonicera japonica Thunb. is a climbing plant that belongs to the genus *Lonicera* in the family Caprifoliaceae. It is commonly found in mountainous areas, sparse forests, rocky areas, along mountain roads, and village fences, and its original habitat is East Asia, mainly distributed in China, Japan, and Korea (Editorial Committee of Flora of China, 1988). The medicinal parts of honeysuckle are its dried flower buds and dried stems, which are commonly used to treat infections, fever, ulcers, swelling, and influenza (Shang *et al.*, 2011;

Received: 06 Apr 2023. Received in revised form: 08 Sep 2023. Accepted: 19 Sep 2023. Published online: 21 Sep 2023.
From Volume 49, Issue 1, 2021, Notulae Botanicae Horti Agrobotanici Cluj-Napoca journal uses article numbers in place of the traditional method of continuous pagination through the volume. The journal will continue to appear quarterly, as before, with four annual numbers.

National Pharmacopoeia Committee, 2020). Recent research has shown that honeysuckle can inhibit influenza A virus and COVID-19 (Zhang *et al.*, 2012; Zhou *et al.*, 2015). Modern research indicates that the main active ingredients of honeysuckle are flavonoids, phenolic acids, and iridoids (Wang *et al.*, 2020; Wang *et al.*, 2023). In addition, honeysuckle is also widely used in cosmetics, food additives, beverages, and landscaping due to its medicinal properties and beautiful flowers (Cao *et al.*, 2022; Ge *et al.*, 2022).

Currently, research on honeysuckle mainly focuses on metabolite analysis (Wang *et al.*, 2023), flower development (Yang *et al.*, 2019), colour changes (Li *et al.*, 2019; Xia *et al.*, 2021), carotenoid metabolism (Pu *et al.*, 2020; Yu *et al.*, 2022), stress (Cai *et al.*, 2022), genome sequencing (Xiao *et al.*, 2021), and effective component biosynthesis pathway (Wang *et al.*, 2020). However, there are few reports on the identification of pigment components, anthocyanin biosynthesis pathways, and regulatory mechanisms of red honeysuckle flower (Yuan *et al.*, 2012; Li *et al.*, 2019).

'Yujin 2' is a superior cultivar of honeysuckle, whose young branches, leaves, flower buds, and corolla are all red. This cultivar has strong resistance to cold and drought, high yield, early flowering, long flowering period, large flower buds, and a strong, non-bitter fragrance (Li *et al.*, 2019; Li *et al.*, 2022). In contrast, another superior honeysuckle cultivar, 'Yujin 1', has green young branches and leaves, and green-white flower buds and corolla. It also has characteristics such as cold and drought resistance, disease and pest resistance, long flowering period, large flower buds, and high yield. Therefore, 'Yujin 2' and 'Yujin 1', the two contrasting cultivars with different flower bud colours, are excellent materials for studying the pigment components, biosynthetic pathway and regulatory mechanism of honeysuckle anthocyanins. Previous studies have shown that the content of chlorophyll and carotenoids in the flower buds of 'Yujin 2' is low, and the high content of anthocyanins is the root cause of its red colour (Yuan *et al.*, 2012; Li *et al.*, 2019).

The anthocyanin biosynthesis and its regulatory mechanism in plants has been extensively studied (LaFountain and Yuan, 2021; Araguirang and Richter, 2022). The pathway originates from the cytosolic phenylpropanoid pathway, where phenylalanine is catalysed by phenylalanine ammonialyase (PAL), cinnamic acid 4-hydroxylase (C4H), and 4-coumarate CoA ligase (4CL) to form p-coumaroyl-CoA. Then, one molecule of p-coumaroyl-CoA and three molecules of malonyl-CoA are catalysed by chalcone synthase (CHS), chalcone isomerase (CHI), flavonoid 3',5'-hydroxylase (F3'5'H), and flavanone-3-hydroxylase (F3H), and flavonoid 3'-hydroxylase (F3'H) to form dihydroquercetin, dihydrokaempferol and dihydromyricetin, respectively. These are the early reaction of anthocyanin synthesis. Then, dihydromyricetin, dihydrokaempferol and dihydroquercetin are catalysed by dihydroflavonol 4-reductase (DFR), anthocyanin synthase (ANS) and anthocyanin: flavonoid glucosyltransferase (UFGT) to generate delphinidin 3-O-glucoside, pelargonidin 3-O-glucoside and cyanidin 3-O-glucoside, respectively. These anthocyanins are further modified by methyltransferase (MT) and acyltransferase (AT) before being transported by glutathione S-transferase (GST) into the vacuole for storage and accumulation. Studies also have shown that almost all flowering plants regulate anthocyanin biosynthesis through a highly conserved MYB-bHLH-WDR (MBW) protein complex (LaFountain and Yuan, 2021; Liu *et al.*, 2021).

With the rapid development of sequencing technology, metabolome and transcriptome have been widely used in the identification of secondary metabolites such as longan anthocyanins (Yi *et al.*, 2021), honeysuckle pigments and aroma (Xia *et al.*, 2021; Li *et al.*, 2022), soapberry triterpenoid Saponin (Xu *et al.*, 2022), and blueberry flavonoids (Wu *et al.*, 2022), as well as the analysis of their biosynthetic pathways and regulatory mechanisms. In this study, we identified the anthocyanins present in flower buds of two varieties using ultra-performance liquid chromatography (UPLC) and electrospray ionization mass spectrometry/mass spectrometry (ESI-MS/MS). Then, we conducted transcriptome sequencing analysis to reveal the biosynthesis pathway and possible regulatory mechanism of anthocyanin in red honeysuckle. Our findings offer valuable insights into the biosynthesis and regulation mechanism of anthocyanins in red honeysuckle.

Materials and Methods

Plant materials

The fresh flower buds of *Lonicera japonica* Thunb. cultivar 'Yujin 1' (LjW, accession: SAMN33906972, SAMN33906973, and SAMN33906974) and 'Yujin 2' (LjR, accession: SAMN33906969, SAMN33906970, and SAMN33906971) at harvesting stage were collected from the Taihefulou Village, Huolong Town, Yuzhou City, Henan Province, China (Figure 1).

Figure 1. Plant materials used for metabolome and transcriptome analysis. (A) and (B) were LjW and LjR samples collected on October 1, 2022, respectively

Sample preparation and extraction

The sample was freeze-dried, ground into powder (30 Hz, 1.5 min) using ball mill (MM400, Retsch, Germany), and stored at -80 °C until needed. 50 mg powder was weighted using electronic balance (AS 60/220.R2, RADWAG, Poland) and extracted with 0.5 mL methanol/water/hydrochloric acid (500:500:1, V/V/V). Then the extract was vortexed for 5 min and ultrasound using ultrasonic cleaner (KQ5200E, Shumei, China) for 5 min and centrifuged using centrifuge (5424R, Eppendorf, Germany) at 12, 000 g under 4 °C for 3 min. The residue was re-extracted by repeating the above steps again under the same conditions. The supernatants were collected, and filtrated through a membrane filter (0.22 μm, Anpel) before LC-MS/MS analysis.

UPLC conditions

The sample extracts were analyzed using an UPLC-ESI-MS/MS system (UPLC, ExionLC™ AD, https://sciex.com.cn/; MS, Applied Biosystems 6500 Triple Quadrupole, https://sciex.com.cn/). The analytical conditions were as follows, UPLC: column, WatersACQUITY BEH C18 (1.7 μm, 2.1 mm×100 mm); solvent system, water (0.1% formic acid): methanol (0.1% formic acid); gradient program, 95:5 (V/V) at 0 min, 50:50 (V/V) at 6 min, 5:95 (V/V) at 12 min, hold for 2 min, 95:5 (V/V) at 14 min; hold for 2 min; flow rate, 0.35 mL/min; temperature, 40 °C; injection volume, 2 μL.

ESI-MS/MS conditions

Linear ion trap (LIT) and triple quadrupole (QQQ) scans were acquired on a triple quadrupole-linear ion trap mass spectrometer (QTRAP), QTRAP® 6500plus LC-MS/MS System, equipped with an ESI Turbo Ion-Spray interface, operating in positive ion mode and controlled by Analyst 1.6.3 software (Sciex). The ESI source operation parameters were as follows: ion source, ESI+; source temperature 550 ℃; ion spray voltage (IS) 5500 V; curtain gas (CUR) was set at 35 psi, respectively. Anthocyanins were analyzed using scheduled multiple reaction monitoring (MRM). Data acquisitions were performed using Analyst v1.6.3 software (Sciex). Multiquant v3.0.3 software (Sciex) was used to quantify all metabolites. Mass spectrometer parameters including the declustering potentials (DP) and collision energies (CE) for individual MRM transitions were

done with further DP and CE optimization. A specific set of MRM transitions were monitored for each period according to the metabolites eluted within this period.

RNA extraction and qualification

The total RNA of LjW and LjR was extracted using the RNAprep Pure Plant Kit (Tiangen, Beijing, China) according the instructions provided by the manufacturer. RNA concentration and purity were measured using NanoDrop 2000 (Thermo Fisher Scientific, Wilmington, DE). RNA integrity was assessed using the RNA Nano 6000 Assay Kit of the Agilent Bioanalyzer 2100 system (Agilent Technologies, CA, USA).

Library preparation and transcriptome sequencing

A total amount of 1 μg RNA per sample was used as input material for the RNA sample preparations. Sequencing libraries were generated using Hieff NGS Ultima Dual-mode mRNA Library Prep Kit for Illumina (Yeasen Biotechnology (Shanghai) Co., Ltd.) following manufacturer's recommendations and index codes were added to attribute sequences to each sample. Briefly, mRNA was purified from total RNA using poly-T oligo-attached magnetic beads. First strand cDNA was synthesized and second strand cDNA synthesis was subsequently performed. Remaining overhangs were converted into blunt ends via exonuclease/polymerase activities. After adenylation of 3' ends of DNA fragments, NEBNext Adaptor with hairpin loop structure were ligated to prepare for hybridization. The library fragments were purified with AMPure XP system (Beckman Coulter, Beverly, USA). Then 3 μl USER Enzyme (NEB, USA) was used with size-selected, adaptor-ligated cDNA at 37 °C for 15 min followed by 5 min at 95 °C before PCR. Then PCR was performed with Phusion High-Fidelity DNA polymerase, Universal PCR primers and Index (X) Primer. At last, PCR products were purified (AMPure XP system) and library quality was assessed on the Agilent Bioanalyzer 2100 system. The libraries were sequenced on an Illumina NovaSeq6000 platform to generate 150 bp paired-end reads, according to the manufacturer's instructions.

Quality control

Raw reads of fastq format were firstly processed through in-house perl scripts. In this step, clean reads were obtained by removing reads containing adapter, reads containing ploy-N and low-quality reads from raw data. At the same time, Q20, Q30, GC-content and sequence duplication level of the clean data were calculated. All the downstream analyses were based on clean data with high quality.

Reads mapping to the reference genome

The adaptor sequences and low-quality sequence reads were removed from the data sets. Raw sequences were transformed into clean reads after data processing. These clean reads were then mapped to the reference genome sequence. Only reads with a perfect match or one mismatch were further analysed and annotated based on the reference genome. Hisat2 v2.04 software was used to map with reference genome assembly ASM2146441v1.

Novel transcripts Prediction

Reference Annotation Based Transcript (RABT) assembly method was used to construct and identify both known and novel transcripts from Hisat2 alignment results using the StringTie v2.2.1 software.

Gene functional annotation

Gene function was annotated based on the following databases: Nr (NCBI non-redundant protein sequences, diamond v2.0.15, parameters: -k 100 -e -evalue 1e-5 -f 5); eggNOR (A database of orthology relationships, functional annotation, and gene evolutionary histories, diamond v2.0.15); KOG/COG (Clusters of Orthologous Groups of proteins, diamond v2.0.15); Swiss-Prot (A manually annotated and

reviewed protein sequence database, diamond v2.0.15); KO (KEGG Ortholog database, diamond v2.0.15); Pfam (Protein family, hmmscan v3.3.2, parameters: --noali --cut_nc --acc --notextw); GO (Gene Ontology, InterProScan v5.34-73.0, parameters: -appl Pfam -goterms -iprlookup -pa -f xml -dp -t p).

Quantification of gene expression levels

Gene expression levels were estimated by fragments per kilobase of transcript per million fragments mapped (FPKM). The formula is shown as follow:

$$\text{FPKM} = \frac{\text{cDNA Fragments}}{\text{Mapped Fragments (Millions)} * \text{Transcript Length (kb)}}$$

Pearson's correlation coefficient r was used to assess the biological replicates' correlation (Liu *et al.*, 2018).

Differential expression analysis

Differential expression analysis of two groups was performed using the DESeq2 v1.30.1 software. DESeq2 provide statistical routines for determining differential expression in digital gene expression data using a model based on the negative binomial distribution. The resulting P values were adjusted using the Benjamini and Hochberg's approach for controlling the false discovery rate. Genes with an adjusted P-value < 0.01 & Fold Change≥2 found by DESeq2 were assigned as differentially expressed.

GO enrichment analysis

Gene Ontology (GO) enrichment analysis of the differentially expressed genes (DEGs) was implemented by the clusterProfiler (Wu *et al.*, 2021) packages based Wallenius non-central hyper-geometric distribution (Young *et al.*, 2010),which can adjust for gene length bias in DEGs.

KEGG pathway enrichment analysis

We used KOBAS (Mao *et al.*, 2005) database and clusterProfiler (Wu *et al.*, 2021) software to test the statistical enrichment of DEGs in KEGG pathways.

Construction of protein protein interaction (PPI)

The sequences of the DEGs was blast (blastx) to the genome of a related species (the protein-protein interaction of which exists in the STRING database: http://string-db.org/) to get the predicted PPI of these DEGs. Then the PPI of these DEGs were visualized in Cytoscape (Shannon *et al.*, 2003).

Splicing event quantification

Different alternative splicing (AS) events were detected and quantified using the rMATS v4.02 software. The number of AS events in each sample was estimated, separately.

Transcription factors prediction

The transcription factors (TFs) were predicted with iTAK v1.6 (Zheng *et al.*, 2016).

Results

Appearance characteristics of honeysuckle flower buds

In general, most varieties of honeysuckle produce yellow-white or green-white flower buds, with reports of red honeysuckle is extremely rare. LjW, one of the more common varieties, produces yellowish-white or

greenish-white, densely villous flower buds (Figure 1A). In contrast, the flower buds of LjR are red and densely pubescent (Figure 1B).

Determination of the main contents of anthocyanins and other flavonoids

To determine the types and components of anthocyanins and other flavonoids in the honeysuckle flower buds of LjW and LjR, we used LC-MS/MS technology for quantitative analysis. Results showed that a total of 59 kinds of anthocyanins (including 10 kinds of cyanidin, 12 kinds of delphinidin, 10 kinds of malvidin, 8 kinds of pelargonidin, 11 kinds of peonidin, and 8 kinds of petunidin), and 5 kinds of flavonoids were identified (Table 1). In the flower bud of LjW, the main anthocyanin components were peonidin-3-O-(6-O-p-coumaroyl)-glucoside (9.21 μg/g) and pelargonidin-3-O-(6-O-p-coumaroyl)-glucoside (7.1193 μg/g), and the main flavonoid components were rutin (1131.05 μg/g), quercetin-3-O-glucoside (294.49 μg/g), and kaempferol-3-O-rutinoside (102.11 μg/g) (Table 1). In the flower bud of LjR, the main anthocyanin components were cyanidin-3,5-O-diglucoside (633.50 μg/g), peonidin-3,5-O-diglucoside (73.94 μg/g) and cyanidin-3-O-glucoside (3.75 μg/g), and the main flavonoid components were rutin (971.78 μg/g), quercetin-3-O-glucoside (344.48 μg/g), and kaempferol-3-O-rutinoside (77.29 μg/g) (Table 1). Therefore, the biosynthesis pathway of cyanidin will be studied in detail.

Table 1. Anthocyanins and other flavonoids detected in LjW and LjR flower buds

Class	Compounds	Q1 (Da)	Q3 (Da)	Molecular weight	Ion mode	LjR (μg/g)	LjW (μg/g)
Cyanidin	Cyanidin-3,5-O-diglucoside	611.2	287.1	611.1612	Positive	633.5035	0.6263
	Cyanidin-3-O-glucoside	449.1	287.1	449.1084	Positive	3.7547	NA
	Cyanidin-3-O-rutinoside	595.17	287.1	595.1663	Positive	0.2263	NA
	Cyanidin-3-(6-O-p-caffeoyl)-glucoside	611.14	287.1	611.1401	Positive	0.0793	0.0201
	Cyanidin-3-O-arabinoside	419.1	287.1	419.0978	Positive	0.0174	0.0129
	Cyanidin-3-O-(6-O-malonyl-beta-D-glucoside)	535.1	287.1	535.1088	Positive	0.0079	0.0072
	Cyanidin-3-O-sambubioside	581.1	287.1	581.1506	Positive	0.0037	0.0042
	Cyanidin-3-O-5-O-(6-O-coumaroyl)-diglucoside	757.2	287.1	757.198	Positive	0.0024	0.0012
	Cyanidin-3,5,3'-O-triglucoside	773.21	287.1	773.214	Positive	NA	0.0007
	Cyanidin-3-O-rutinoside-5-O-glucoside	757.22	287.1	757.2191	Positive	NA	0.0014
Delphinidin	Delphinidin-3-O-glucoside	465.1	303.1	465.1033	Positive	0.5803	0.1966
	Delphinidin-3-O-galactoside	465.1	303.1	465.1033	Positive	0.2212	0.0715
	Delphinidin-3-O-rutinoside-5-O-glucoside	773.21	303.1	773.214	Positive	0.1329	0.0862
	Delphinidin-3-O-sophoroside	627.15	303.1	627.1561	Positive	0.0889	0.0429
	Delphinidin-3-O-rutinoside	611.1	303.1	611.1612	Positive	0.0426	0.0252
	Delphinidin-3-O-sambubioside	597.1	303.1	597.1456	Positive	0.0133	0.0029
	Delphinidin-3-O-(6-O-acetyl)-glucoside	507.11	303.1	507.1139	Positive	0.0119	0.0069
	Delphinidin	303.1	149	303.0505	Positive	0.007	0.0044
	Delphinidin-3-O-5-O-(6-O-coumaroyl)-diglucoside	773.19	303.1	773.1929	Positive	0.0031	NA
	Delphinidin-3-O-(6-O-malonyl)-glucoside-3'-glucoside	713.16	303.1	713.1565	Positive	0.0021	0.0016
	Delphinidin-3-O-(6-O-p-coumaroyl)-glucoside	611.14	303.1	611.1401	Positive	NA	0.011
	Delphinidin-3-O-rhamnoside	449.1	303.1	449.1084	Positive	NA	0.0105
Malvidin	Malvidin-3,5-O-diglucoside	655.4	331.1	655.1874	Positive	0.0077	0.0592
	Malvidin-3-O-arabinoside	463.3	331.06	463.124	Positive	NA	0.0437
	Malvidin-3-O-rutinoside	639.06	331.1	639.1925	Positive	0.0124	0.0386
	Malvidin-3-O-(6-O-p-coumaroyl)-glucoside	639.17	331.1	639.1714	Positive	NA	0.0343
	Malvidin-3-O-(6''-acetylglucoside)-5-glucoside	697.2	331.1	697.198	Positive	NA	0.0263
	Malvidin-3-O-sambubioside	625.19	331.1	625.1769	Positive	0.0063	0.0113
	Malvidin-3-O-glucoside	493.1	331.1	493.1346	Positive	NA	0.006
	Malvidin-3-O-5-O-(6-O-coumaroyl)-diglucoside	801.22	331.1	801.2242	Positive	NA	0.0014
	Malvidin-3-O-sambubioside-5-O-glucoside	787.4	331.3	787.2297	Positive	0.001	0.0013
	Malvidin-3-O-galactoside	493.2	331.1	493.1346	Positive	NA	NA
Pelargonidin	Pelargonidin-3-O-(6-O-p-coumaroyl)-glucoside	579.15	271.1	579.1503	Positive	NA	7.1193
	Pelargonidin-3-O-galactoside	433.2	271.1	433.1135	Positive	0.015	0.0206
	Pelargonidin-3-O-sambubioside	565.2	271.1	565.1557	Positive	0.003	0.0023
	Pelargonidin-3-O-sophoroside	595.14	271.1	595.1663	Positive	0.0038	0.0021
	Pelargonidin-3-sophoroside-5-glucoside	757.22	271.1	757.2191	Positive	0.0008	0.0008

	Pelargonidin-3,5-O-diglucoside	595.1	271.1	595.1663	Positive	0.8958	NA
	Pelargonidin-3-O-glucoside	433.2	271.1	433.1135	Positive	0.0366	NA
	Pelargonidin-3-O-rutinoside-5-O-glucoside	741.22	271.1	741.2242	Positive	0.001	NA
Peonidin	Peonidin-3,5-O-diglucoside	625.2	301.1	625.1769	Positive	73.9349	NA
	Peonidin-3-O-(6-O-p-coumaroyl)-glucoside	609.16	301.1	609.1608	Positive	0.3394	9.205
	Peonidin-3-O-glucoside	463.3	301.1	463.124	Positive	0.2494	NA
	Peonidin-3-O-galactoside	463.3	301.1	463.124	Positive	0.102	NA
	Peonidin-3-O-sophoroside	625.1	301.1	625.1769	Positive	0.0183	0.0141
	Peonidin-3-O-rutinoside	609.5	301.1	609.1819	Positive	0.0122	NA
	Peonidin-3-O-sambubioside-5-O-glucoside	757.23	301.1	757.2191	Positive	0.0088	NA
	Peonidin-3-O-sambubioside	595.19	301.1	595.1663	Positive	0.0041	NA
	Peonidin-3-sophoroside-5-glucoside	787.23	301.1	787.2297	Positive	0.0028	NA
	Peonidin-3-O-(6-O-malonyl-beta-D-glucoside)	549.5	301.1	549.1244	Positive	0.0018	0.0031
	Peonidin-3-O-5-O-(6-O-coumaroyl)-diglucoside	771.21	301.1	771.2136	Positive	0.0016	0.0031
Petunidin	Petunidin-3-O-sambubioside	611.15	317.1	611.1612	Positive	NA	0.0116
	Petunidin-3-O-sambubioside-5-O-glucoside	773.2	317.1	773.214	Positive	NA	0.0044
	Petunidin-3-O-galactoside	479.1	317.1	479.119	Positive	0.0208	0.0377
	Petunidin-3-O-rutinoside	625.06	317.1	625.1769	Positive	0.0082	0.0082
	Petunidin-3-O-sophoroside	641.11	317.1	641.1718	Positive	0.0029	0.0028
	Petunidin-3-O-(6-O-p-coumaroyl)-glucoside	625.18	317.1	625.1557	Positive	0.0023	NA
	Petunidin-3,5-O-diglucoside	641.2	317.1	641.1718	Positive	0.0014	0.001
	Petunidin-3-O-5-O-(6-O-coumaroyl)-diglucoside	787.21	317.1	787.2086	Positive	0.001	0.0011
Flavonoid	Rutin	611.2	303.1	610.1534	Positive	1131.0467	971.7750
	Quercetin-3-O-glucoside	465.1	303.1	464.0955	Positive	294.4945	344.4793
	Kaempferol-3-O-rutinoside	595.2	287.1	594.1585	Positive	102.1172	77.2855
	Naringenin-7-O-glucoside	435.1	273.1	434.1213	Positive	0.7853	0.9991
	Afzelin	433.1	287.1	432.1056	Positive	0.1362	0.2231

*Notes: NA represents not detect

Sequencing, assembly and annotation

To identify key candidate genes of anthocyanin biosynthesis pathway, RNA sequencing was performed using the flower buds LjW (LjW1, LjW2, and LjW3) and LjR (LjR1, LjR2, and LjR3). Six cDNA libraries were sequenced, and after data filtering, each sample generated over 19,668,207 clean reads, with Q20 and Q30 values greater than 97.45% and 92.90%, separately. The clean reads obtained from each sample ranged from 5.80 to 6.70 Gb (Table 2), which have been deposited in the Short Reads Archive (SRA) database under accession number: PRJNA948551.

Table 2. Quality assessment of the sequencing data

Sample	Clean reads	Clean bases	GC (%)	Q20 (%)	Q30 (%)
LjR1	22,430,399	6,715,212,210	44.36%	97.68	93.42%
LjR2	21,382,613	6,401,061,708	44.57%	97.70	93.47%
LjR3	21,026,606	6,293,408,696	44.38%	97.72	93.49%
LjW1	21,879,624	6,548,751,990	44.51%	97.59	93.23%
LjW2	20,531,504	6,146,687,976	44.33%	97.59	93.15%
LjW3	19,668,207	5,888,194,678	44.52%	97.45	92.90%

All clean reads were aligned to the reference genome of *L. japonica*, and a majority of the LjR (92.67-94.13%) and LjW (95.90-96.32%) sequences were mapped to the reference genome (Table S1). These results suggested that our data was reliable. We used the Stringtie software (Pertea *et al.*, 2015) to assemble the transcripts, and unigenes that were detected in the sequencing results but were absent in the reference genome were classified as novel genes. Our analysis identified a total of 7609 novel genes, with 6313 genes (82.97% of novel genes) detected in LjW, and 7006 genes (92.08% of novel genes) detected in LjR.

To annotate the assembled genes, we utilized BLASTX with an E-value threshold of 10^{-5}, against several public databases including Nr, eggNOR, GO, Pfam, Swiss-Prot, KOG, and KEGG. A total of 35,687 assembled unigenes were successfully annotated (Table S2). Based on sequence similarity, 29,296 (32.40%) unigenes were

classified into three groups (biological process, cellular component and molecular function) using GO term analysis (Figure S1). The biological processes were predominantly associate with "cellular process (12835, 43.81%)" and "metabolic process (12069, 41.20%)". The cellular components were primarily related to "cellular anatomical entity (15195, 51.87%)". The molecular functions were mainly classified into "binding (15320, 52.29%)" and "catalytic activity (14108, 48.16%)". KEGG enrichment analysis was utilized to identify the functional pathways of the unigenes. Of the total unigenes, 24,501 (59.00%) unigenes were significantly enriched in 137 KEGG pathways, with "plant-pathogen interaction (1613, 6.58%)" being the largest group, followed by "plant hormone signal transduction (878, 3.58%)", "protein processing in endoplasmic reticulum (609, 2.49%)", "MAPK signaling pathway-plant (594, 2.42%)", "starch and sucrose metabolism (551, 2.25%)" and "phenylpropanoid biosynthesis (534, 2.18%)" (Figure S2).

Analysis of gene expression

The correlation of gene expression levels among samples is a crucial indicator for testing the repeatability of biological experimental operations, evaluating the reliability of DEGs, and assisting in the screening of abnormal samples. To assess the biological replicates' correlation, we employed Pearson's correlation coefficient r as the evaluation index(Liu *et al.*, 2018). In this study, we observed that the correlation coefficient between the LjR samples was greater than 0.93, while it was greater than 0.82 for the LjW samples, indicating stronger correlation among duplicate samples (Figure 2).

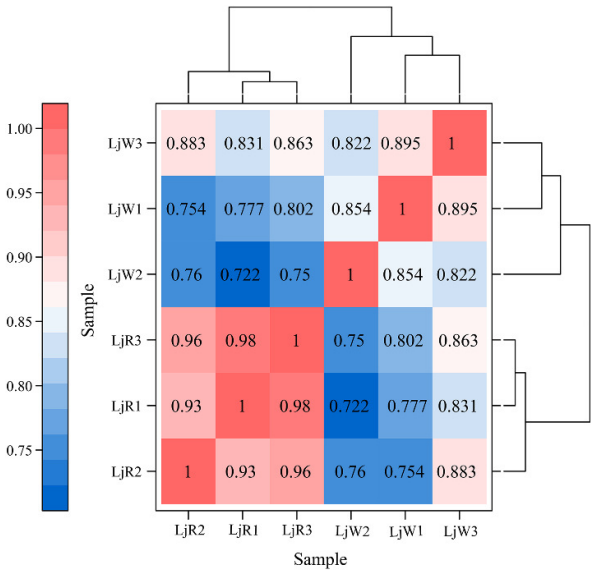

Figure 2. Correlation heat map of expression quantity of two samples. The values on each colour block on the heatmap represent the correlation between the two samples on the horizontal and vertical axis corresponding to the colour block

The higher the value, the stronger the correlation.

Principal component analysis (PCA) can reduce multiple variables into a few independent variables (i.e. principal components). In transcriptome analysis, the gene expressions are reduced to find the rule of sample distribution from complex data, allowing for the evaluation of sample dispersion. The closer the points in the PCA diagram, the more similar the composition. As shown in Figure 3, PCA results showed that the three samples of LjW had similar compositions, so did the samples of LjR.

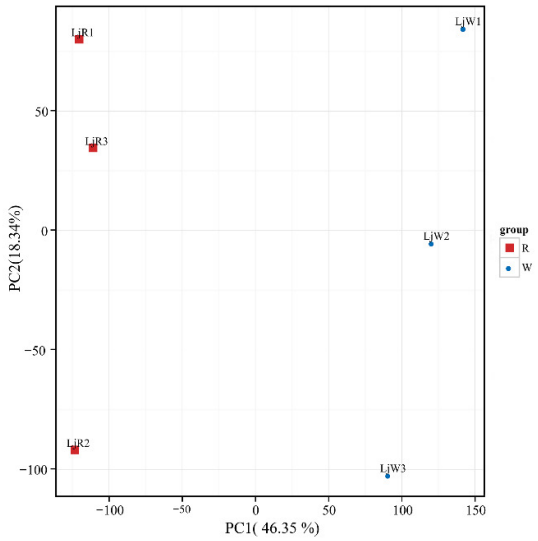

Figure 3. The results of PCA analysis. The coordinates indicate different principal components, while the corresponding percentage values represent the contribution of these principal components to the differences observed within the samples

Each point on the graph represents a sample, with those belonging to the LjR and LjW groups denoted by red squares and blue dots, respectively.

Identification and analysis of DEGs

Transcriptomic analyses were performed on honeysuckles to identify the key DEGs between the W (LjW) and R (LjR) groups. A total of 4,436 DEGs were obtained, consisting of 1,481 upregulated genes and 2,955 downregulated genes in W vs. R. The DEGs were identified using a threshold of |Fold Change| ≥2 and a false discovery rate (FDR) of less than 0.01 (Figure 4).

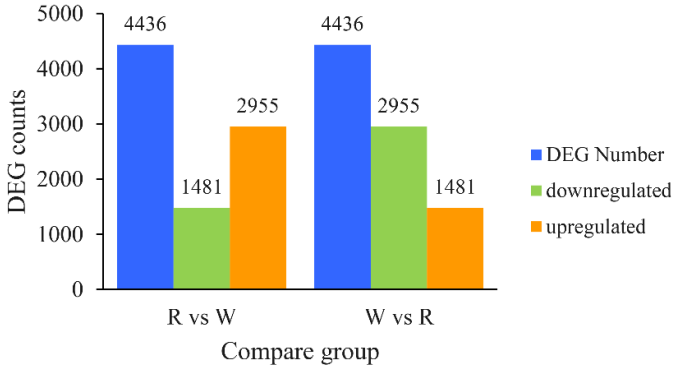

Figure 4. Histogram of DEGs statistics. The x-axis indicates the various sets of DEGs, with blue representing all DEGs, orange representing upregulated genes, and green representing downregulated genes

The y-axis indicates the number of DEGs in each set.

To investigate potential functional relationships between DEGs, hierarchical clustering analysis was performed on all screened DEGs. Genes with similar expression patterns are often associated with similar functions. The analysis aimed to display expression differences among the genes in different groups and identify novel functional genes. As shown in Figure 5, the upregulated genes in LjR were clustered in the upper right region of the heatmap, indicating a close association with the red phenotype.

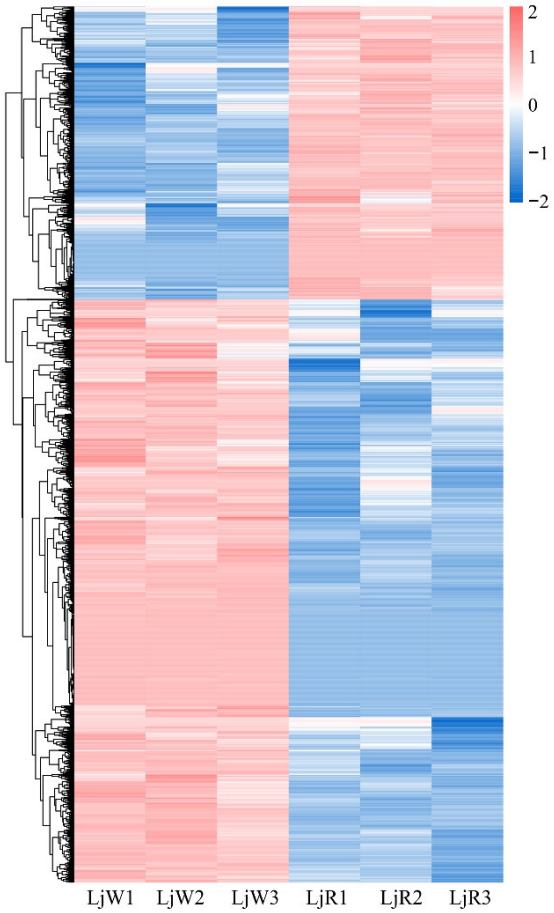

Figure 5. Cluster diagram of DEGs. The x-axis indicates the sample name, while the y-axis indicates the clustering result of the DEGs. Each column in the figure represents a different sample, and each row represents a different gene

The colour scheme represents the level of gene expression in log10(FPKM+1) for each sample.

Enrichment analysis of DEGs

To gain insights into the potential functions of the DEGs, we performed differential GO clustering analysis focusing on three major categories: cellular component, biological process, and molecular function. Our analysis revealed that 1329 unigenes were associated with the metabolic process in the biological process category, while 1445 unigenes showed catalytic activity in the molecular function category (Figure 6).

In total, we annotated 2612 genes for 125 KEGG metabolic pathways in the two cultivars. Among them, 810 unigenes (31.01%) were found to be involved in the metabolic pathway. We identified 8 significantly enriched metabolic pathways with a q value < 0.05, including "photosynthesis-antenna proteins", "starch and sucrose metabolism", "ascorbate and aldarate metabolism", "cyanoamino acid metabolism", "photosynthesis", "flavonoid biosynthesis", "phenylpropanoid biosynthesis", and "flavone and flavonol biosynthesis". Notably, "flavonoid biosynthesis (ko00941, 36 DEGs)" and "flavone and flavonol biosynthesis (ko00944, 9 DEGs)" showed significant enhancement (Figure 7).

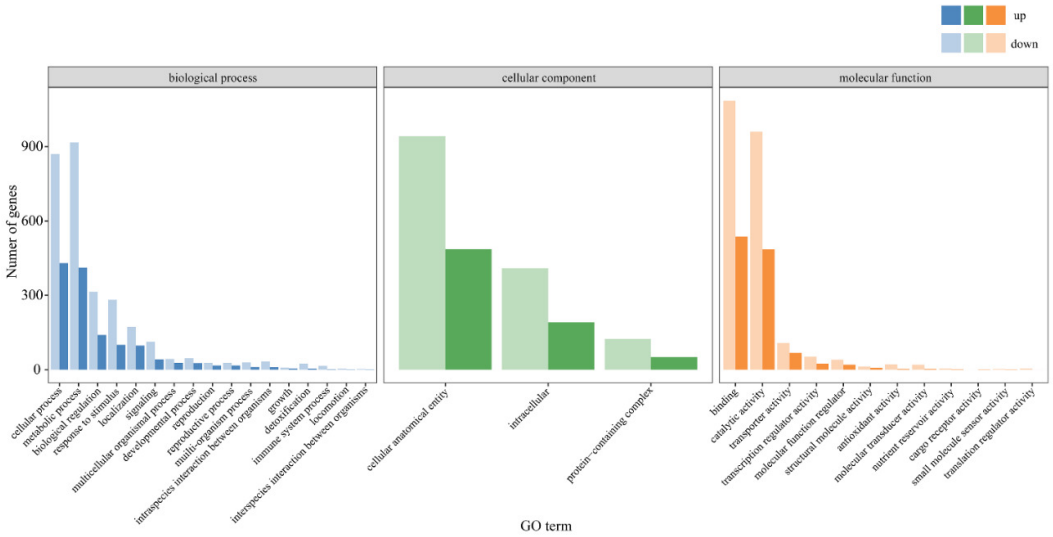

Figure 6. Histogram of GO enrichment of DEGs. The y-axis represents the number of genes annotated in each GO entry, while the x-axis indicates the different GO entries
The colour of each column indicates the q value of the hypergeometric test for GO enrichment.

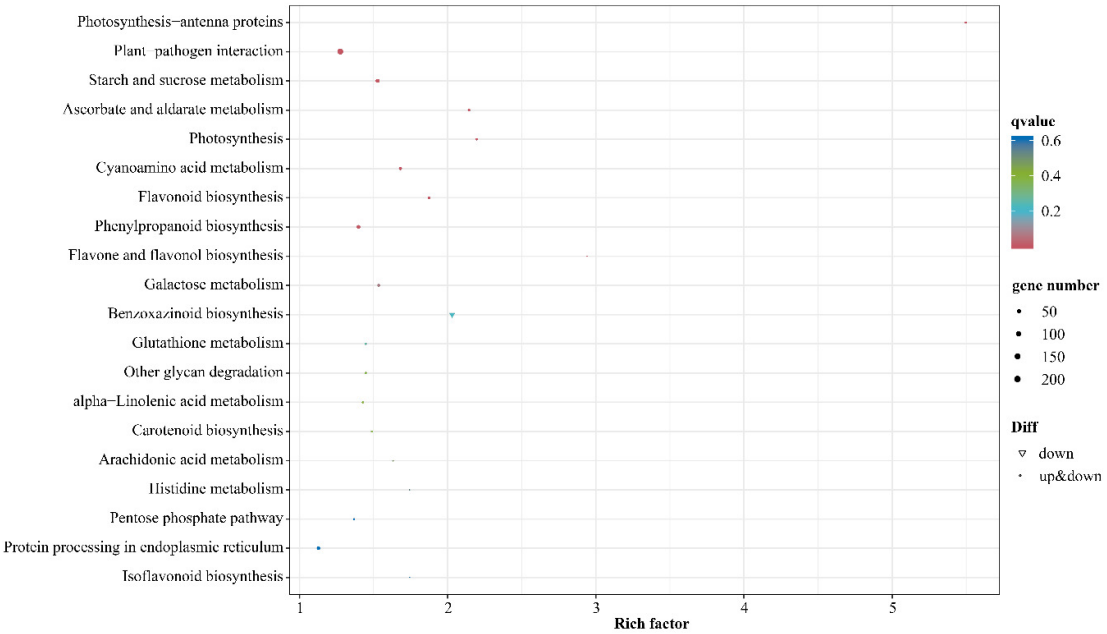

Figure 7. Bubble diagram of KEGG enrichment of DEGs. Each circle represents a KEGG pathway. The pathway name is on the ordinate, and the abscissa indicates the rich factor, representing the ratio of the proportion of genes annotated to a pathway in the differential gene to the proportion of genes annotated to the pathway in all genes. The larger the enrichment factor, the more significant the enrichment level of DEGs in this pathway. The colour of the circle represents the q-value, which is the p-value corrected by multiple hypothesis tests. The smaller the q-value, the more reliable the enrichment significance of DEGs in the pathway. The size of the circle indicates the number of genes enriched in the pathway, with a larger circle indicating more genes in the pathway. The circle's position in the upper right corner indicates its higher reference value.

Analysis of structural genes involved in anthocyanin biosynthesis

We constructed an anthocyanin biosynthesis pathway in honeysuckle based on the pathway reported in plants (Khan *et al.*, 2022)(Figure 8). The pathway comprises of structural genes, such as *PAL*, *C4H*, and *4CL*, which are involved in phenylpropanoid biosynthesis, and *CHS*, *CHI*, *F3H*, *F3'H*, *F3'5'H*, *DFR*, *ANS*, *UFGT*, *MT*, and *AT*, which are involved in anthocyanin biosynthesis. Multiple copies of these genes were found, and some exhibited significantly higher expression levels in LjR than in LjW. Specifically, the expression levels of *4CL1* and *4CL4*, *CHS2*, *CHS3*, *CHS4*, *F3H1*, *F3'H*, *DFR1*, *ANS2*, *ANS3*, *UFGT4* and *UFGT8* genes were much higher in LjR flower buds than in LjW (Figure 8). Enzyme genes at the brunching point, *FLS4* and *ANR4*, also showed significantly higher expression levels in LjR than in LjW (Figure 8).

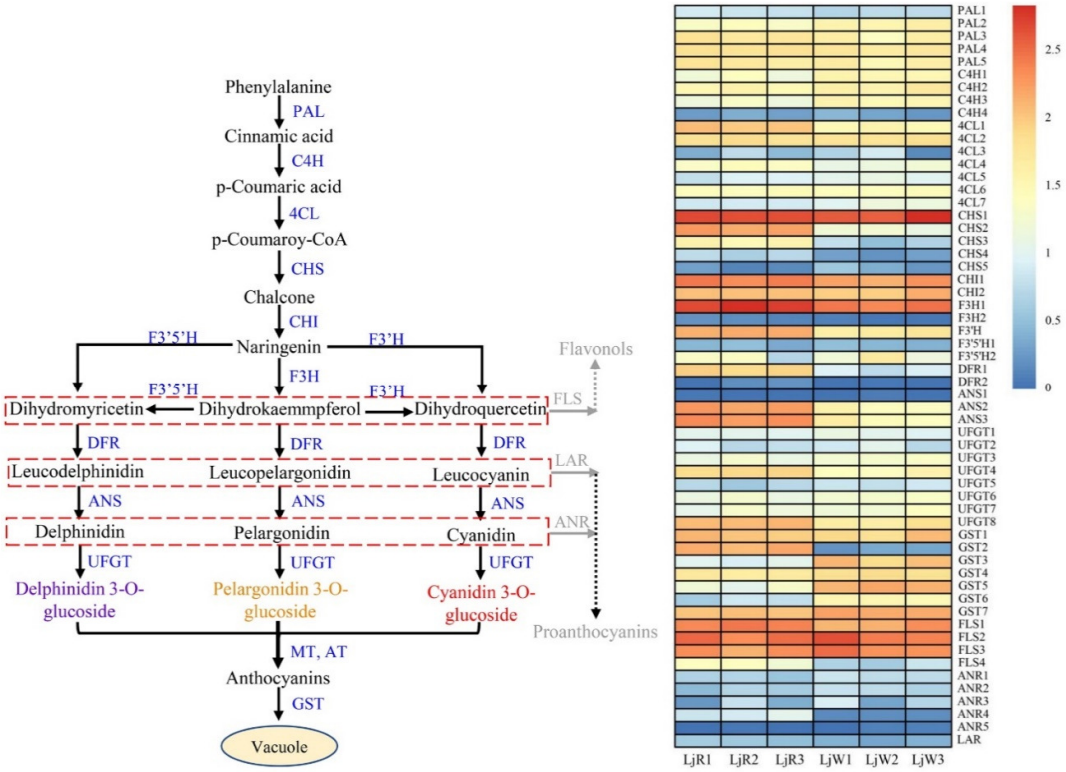

Figure 8. Proposed pathway of anthocyanin biosynthesis and structural gene expression in honeysuckle (A) The putative biosynthetic pathway of anthocyanin. The arrows denote the deduced reactions of anthocyanin. (B) Heatmap based on expression level of genes involved in anthocyanin biosynthesis between LjR and LjW. The expression level was calculated as FPKM value for each gene, and log10 (FPKM + 1) was used to plot the heatmap. Candidate genes come from the annotations. The heatmap represents the expression levels of structural genes, with blue indicating low expression levels and red indicating high expression levels. The enzymes in this pathway are: PAL, phenylalanine ammonia lyase; C4H, cinnamate 4-hydroxylase; 4CL, 4-coumarate CoA ligase; CHS, chalcone synthase; CHI, chalcone isomerase; F3H, flavanone 3-hydroxylase; F3'H, flavonoid 3'-hydroxylase; F3'5'H, flavonoid 3', 5'-hydroxylase; DFR, dihydroflavonol 4-reductase; ANS, anthocyanidin synthase; UFGT, UDP-glucose: flavonoid 3-O-glucosyltransferase; GST, glutathione S-transferase; MT, methyl transferase; AT, acyl transferase; FLS, flavonol synthase; LAR, leucoanthocyanidin reductase.

The conversion of naringenin to dihydrokaempferol, a necessary step in the production of various anthocyanins, is facilitated by the *F3H* gene. We identified two *F3H* genes using the transcriptome data, with *F3H1* showing strong expression in LjR while F3H2 was expressed at low levels in both LjR and LjW (Figure 8). The *F3'5'H* and *F3'H* genes determine the type of anthocyanin that will be formed (Yi *et al.*, 2021), and we found two *F3'5'H* genes expressed similarly in LjR and LjW, while one F3'H gene was upregulated in LjR

(Figure 8). Therefore, the differential expression of F3′H may be a crucial factor in determining the type of anthocyanins formed.

DFR is a critical enzyme in anthocyanin production with varying catalytic properties for diverse substrates (Wang *et al.*, 2022). We discovered one *DFR* gene (*DFR1*) and two *ANS* genes (*ANS2* and *ANS3*) that were significantly expressed in LjR (Figure 8). The final essential enzymes in anthocyanin biosynthesis are UFGTs, which catalyze the conversion of unstable anthocyanins into stable ones. Two *UFGT* genes (*UFGT4* and *UFGT8*) were upregulated in LjR, but the expression of the other five *UFGT* genes remained unchanged in both LjR and LjW (Figure 8). GSTs prevent flavonoid oxidation or direct them into vacuoles (Lu *et al.*, 2021). We observed that six *GST* genes were downregulated in LjR, and only one *GST* gene (*GST2*) was upregulated (Figure 8).

Identification of TFs related to anthocyanin biosynthesis

Anthocyanin biosynthesis in plant is primarily regulated by the MBW protein complex and other TFs (Cui *et al.*, 2021; LaFountain and Yuan, 2021). In this study, we identified several TFs in honeysuckle, with the top four in quantity being ERF (156), MYB (137), NAC (125), and bHLH (111), as shown in Figure S3. We constructed phylogenetic trees of the MYB and bHLH TFs to compare upregulated and downregulated candidate genes with known genes related to anthocyanin biosynthesis in other plants (Figure 9A and 9B). Based on our analysis, we retrieved 12 MYB, 5 MYB-related, and 6 bHLH TFs (Figure 9C). We proposed that LjMYB112, MYB-related66, LjbHLH20, and LjbHLH23 were potential positive regulators of anthocyanin biosynthesis, while LjMYB49, LjMYB70, LjMYB107, LjMYB75, LjMYB111, LjMYB13, LjMYB54, MYB-related34, MYB-related36, and MYB-related42 were negative regulators (Figure 9). These findings suggest that a complex regulatory network control anthocyanin biosynthesis in honeysuckle flower buds.

In addition to MYB and bHLH TFs, other TFs such as NAC (Zhou *et al.*, 2015; Sun *et al.*, 2019; Zhang *et al.*, 2020), MADS (Li *et al.*, 2021; Qi *et al.*, 2022), ERF (Ni *et al.*, 2019; An *et al.*, 2020), WRKY (Zhou *et al.*, 2015; An *et al.*, 2019), and bZIP (Wang *et al.*, 2022; Liu *et al.*, 2023) were also identified from the DEGs (Figure 9D), consistent with previously reports [19–22]. These TFs may also play a role in regulating the structural and regulatory genes involved in anthocyanin biosynthesis. Our identification of these TFs provides valuable information for future studies on the regulatory mechanisms underlying anthocyanin biosynthesis in honeysuckle.

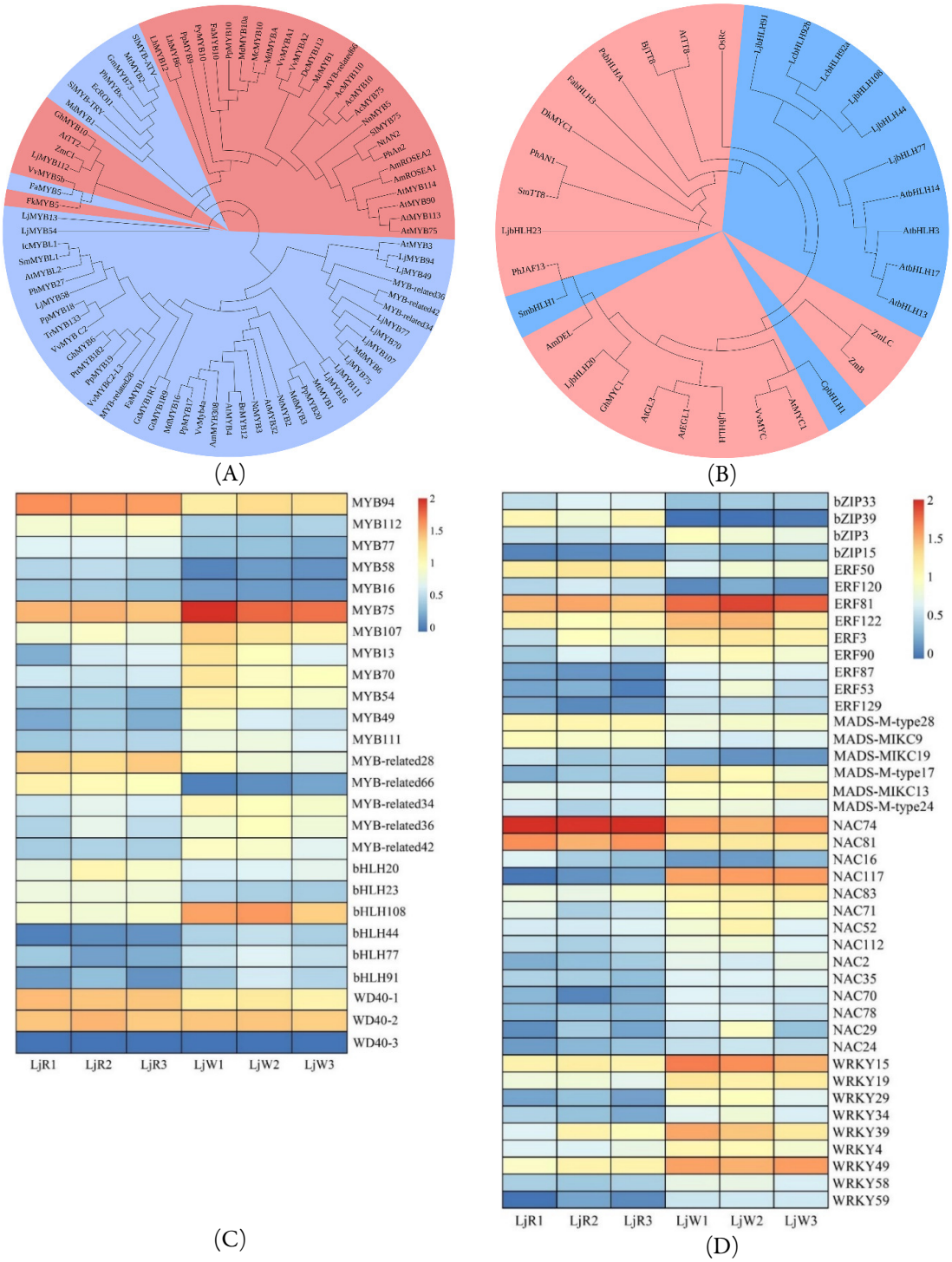

Figure 9. Phylogenetic analysis and expression level of TFs in honeysuckle flower buds
(A) and (B) The phylogenetic analysis of MYBs and bHLHs, respectively. (C) Heatmap based on expression levels of MYB, bHLH, and WD40 in flower buds of LjR and LjW. (D) Heatmap based on expression levels of bZIP, ERF, MADS, NAC, and WRKY in flower buds of LjR and LjW. The expression level for each gene was represented by the FPKM value, and $\log_{10}$ (FPKM + 1) was used to plot the heatmap. Candidate genes were selected based on the annotations. The sequences used for analysis are listed in Supplementary file 1 and Supplementary file 2.

Analysis of PPI network

The PPI network analysis revealed that LjDFR1 is the central hub protein in anthocyanin biosynthesis (Figure 10). LjbHLH23, in conjunction with the bHLH binding protein, was found to act as a positive regulator for the expression of DFR1 (Figure 10). Moreover, LjCHS4 and LjF3H2 were identified as the substrates suppliers for LjDFR1, while LjDFR1 could provide substrates for LjANS2 and LjANS3.

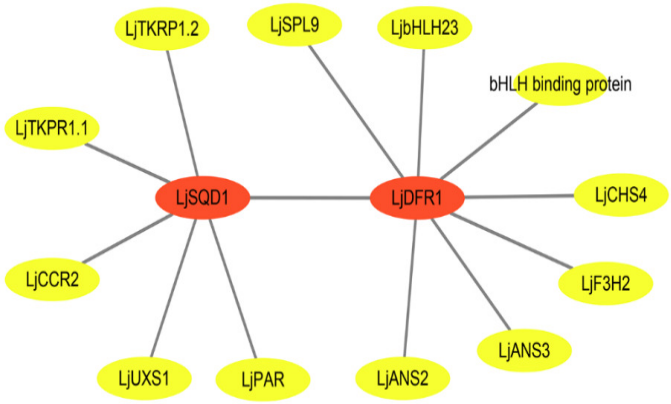

Figure 10. PPI network diagram of DEGs

The nodes in the graph represent proteins, and the edges represent their interactions. The diagram includes several proteins, such as SPL9: Squamosa promoter-binding-like protein 9; SQD1: UDP-sulfoquinovose synthase; UXS1: UDP-glucuronic acid decarboxylase 1; PAR: Phenylacetaldehyde reductase; TKPR1: Tetraketide alpha-pyrone reductase 1; CCR2: Cinnamoyl-CoA reductase 2.

Discussion

The flower buds of honeysuckle contain high levels of flavonoids, phenolic acids, and iridoid compounds, which exhibit anti-inflammatory, antiviral, antioxidant, anticancer, and analgesic effects (Oboh *et al.*, 2013; Han *et al.*, 2016; Kou *et al.*, 2022). These compounds make honeysuckle a valuable resource for various applications, including medicines, food additives, beverages, cosmetics, and landscaping (Xiao *et al.*, 2021). Among the different subspecies of honeysuckle, red honeysuckle has been found to contain higher levels of active substances such as chlorogenic acid, luteoloside, caffeic acid, quercetin, and octylacetate when compared to other varieties (Yuan *et al.*, 2012). Hence, red honeysuckle has greater potential for development and utilization in the food, medicine, cosmetics, and health products industries. In this study, anthocyanin metabolomics analysis identified a total of 59 anthocyanins from two species of honeysuckle, including cyanidin, delphinidin, malvidin, pelargonidin, peonidin, and petunidin. The primary components found in red honeysuckle were cyanidin-3,5-O-diglucoside (633.50 μg/g), peonidin-3,5-O-diglucoside (73.94 μg/g), and cyanidin-3-O-glucoside (3.75 μg/g) (Table 1). These findings provide a scientific basis for further research and development of functional products derived from red honeysuckle.

There are three major types of plant pigments, namely anthocyanins, carotenoids, and chlorophylls. Among these, anthocyanins are the primary pigments responsible for the colour of flowering plants (Khan *et al.*, 2022). Research has shown that anthocyanins possess antioxidant, anti-inflammatory, and other health-promoting properties (Reis *et al.*, 2016). Despite of their potential benefits, there have been limited studies on the red honeysuckle flower (Yuan *et al.*, 2012; Li *et al.*, 2019). To address this gap in knowledge, we utilized metabolomic techniques to obtain detailed information on the six anthocyanin components and their concentrations in the flower buds of two honeysuckle species. Our findings revealed that the cyanidin derivative cyanidin-3,5-O-diglucoside was a common pigment found in both honeysuckle flower buds, with a

content that was approximately 1000 times higher in the LjR flower bud than in the LjW flower bud. Furthermore, cyanidin-3-O-glucoside (3.75 μg/g), cyanidin-3-O-rutinoside (0.22 μg/g), and peonidin-3,5-O-diglucoside (73.93 μg/g) were present only in LjR. Similarly, pelargonidin-3,5-O-diglucoside (0.90 μg/g) was present only in LjR, while pelargonidin-3-O-(6-O-p-coumaroyl)-glucoside (7.12 μg/g) was found only in LjW. Delphinidin-3-O-glucoside was a common pigment in both LjR (0.58 μg/g) and LjW (0.20 μg/g), but the content of the former was about three times higher than that of the latter. In contrast, malvidin derivatives could only be detected in trace amounts in both LjR and LjW. Anthocyanins, the pigments responsible for the red colour in plants, consist of various components that differ from plant to plant. For example, in red apples and red pears, the main pigment component is cyanidin-3-O-galactoside, accounting for more than 80% (Zhang *et al.*, 2012; Chen *et al.*, 2021). Meanwhile, pelargonidin-3-O-glucoside and pelargonidin-3-O-rutoside are the primary pigment components found in strawberries (da Silva *et al.*, 2007). In red peel longan, cyanidin 3-O-glucoside, cyanidin 3-O-6''-malonyl-glucoside, and cyanidin O-symmetric acid are the primary pigment components, as reported by another study (Yi *et al.*, 2021). Thus, the vibrant red colour of LjR honeysuckle is due to the high concentration of cyanidin-3,5-O-diglucoside, which is its primary pigment component.

The anthocyanin biosynthetic pathway is one of the most clearly studied plant secondary metabolic pathways so far. This pathway includes three enzymes in the phenylpropanoid pathway (PAL, C4H and 4CL), early biosynthetic enzymes of anthocyanins (CHS, CHI, F3H, F3'H, F3'5'H) and late biosynthetic enzymes (DFR, ANS, UFTG, MT, AT). In this study, we found that the expression levels of *F3'H*, *DFR*, *ANS2*, *ANS3*, *UFGT4*, and *UFGT8* genes in LjR were significantly higher than those in LjW. The *F3'H* gene, which encodes flavonoid 3'-hydroxylase, is a key gene in the anthocyanin biosynthesis pathway. It catalyses the conversion of dihydrokaempferol to dihydroquercetin. Studies on Arabidopsis mutants have shown that a decrease in *F3'H* gene expression leads to a decrease in anthocyanin content in leaves, stems and other tissues. Overexpression of apple *MdF3'HI* and *MdF3'HIIb* in Arabidopsis *tt7-1* mutant restore its wild type and in wild-type tobacco leads to enhanced red flower colour intensity, respectively (Han *et al.*, 2010). Furthermore, a 6 bp insertion in the *F3'H* gene disrupted its enzymatic activity and hindered cyanidin−/peonidin-type anthocyanin biosynthesis, resulting in a severe reduction of pigment in tree peony (Zhang *et al.*, 2020). Therefore, the high expression of *F3'H* gene in the LjR observed in our study can provide more raw material dihydroquercetin for the biosynthesis of cyanidin. Dihydrokaemmpferol is an important precursor and a key branch point of different types of anthocyanin biosynthesis. Thus, our findings suggest that the high expression of the *F3'H* gene in LjR plays a crucial role in determining the higher concentration of anthocyanins in LjR compared to LjW.

DFR is also a key enzyme gene in the plant anthocyanin biosynthesis pathway, which plays an important role in flower colour development. DFR belongs to the family of reduced coenzyme II (nicotinamide adenine dinucleotide phosphate, NADPH)-dependent short-chain reductases, encoded by single or multiple genes. This enzyme reduces dihydromyricetin flavones, dihydroquercetin, and dihydrokaempferol to their corresponding leucocyanidins by NADPH (Petit *et al.*, 2007). These three substrates of DFR are very similar in structure, differing only in the number of hydroxyl groups on the B benzene ring, which is not the site of enzymatic action. Thus, DFRs from many species utilize all three substrates (Johnson *et al.*, 2001). In *Gerbera jamesonii*, a single amino acid change in the *GjDFR* enzyme can alter the substrate specificity of DFR (Johnson *et al.*, 2001). In purple potatoes, whose *IbDFR* is able to complement the Arabidopsis *tt3* (*dfr*$^{-}$) mutant, downregulation of its expression using RNAi approach diverted the metabolic pathway to the flavonol pathway, resulting in reduced anthocyanin accumulation in young leaves, stems and storage roots (Wang *et al.*, 2013). Therefore, differences in the expression of *DFR* genes and their substrate specificity will lead to flower colour changes. In this study, two *DFR* genes were found, the expression level of *DFR1* gene in LjR was much higher than that in LjW, and the expression level of *DFR2* gene in both was lower. Therefore, we speculate that *DFR1* plays an important role in the coloration of LjR.

The ANS gene is essential for the later stages of anthocyanin biosynthesis, as it encodes an enzyme that converts leucocyanidins to coloured anthocyanins using Fe^{2+} and 2-oxoglutarate. Previous studies have demonstrated that ANS is typically encoded by a small gene family in many plants (Zhao and Tao, 2015). For instance, in pomegranate, insertional mutation in the coding region of the ANS gene can result in enzyme inactivation, leading to the emergence of a white pomegranate phenotype without any anthocyanins present in young leaves, flowers, pericarp, and pulp (Ben-Simhon *et al.*, 2015). In this study, three ANS genes were identified, and it was observed that the expression levels of *ANS2* and *ANS3* genes were significantly higher in LjR than in LjW. Moreover, the expression levels of the *ANS1* gene were lower in both. These findings suggest that genetic differences exist in anthocyanin biosynthesis between these plant species and imply that the regulation of *ANS* gene expression may play a crucial role in determining the colour variation between LjR and LjW.

UFGT is a vital enzyme gene in the late stage of anthocyanin biosynthesis and is responsible for glycosylating anthocyanins to enhance their stability (Muhammad *et al.*, 2022). UFGT has been shown to regulate anthocyanin biosynthesis during litchi fruit coloration (Zhao *et al.*, 2012). Studies on Japanese apricot have revealed that the UFGT activity is higher in safflower than that in white flowers and that it increases as the petals turn red, in parallel with anthocyanins accumulation (Wu *et al.*, 2017). In this study, multiple *UFGT* genes were identified, and the expression levels of *UFGT4* and *UFGT8* genes were found to be much higher in LjR than in LjW. Conversely, GST act as an anthocyanin transporter in both fruits and leaves. This study identified seven *GST* genes, it was observed that the expression levels of *GST1* and *GST2* genes were much higher in LjR than in LjW. Similarly, the expression levels of *GST3*, *GST5*, *GST6*, and *GST7* were higher in LjW, indicating that GST alone cannot account for the observed colour variation between LjW and LjR.

Aside from structural genes in the anthocyanin biosynthetic pathway, TFs can also play a critical role in flower colour development by controlling the spatial and temporal expression of structural genes. The MBW complex is known to regulate plant anthocyanin biosynthesis (Albert *et al.*, 2014; Lloyd *et al.*, 2017). In this study, 12 MYB, 5 MYB-related, and 6 bHLH TFs were identified among the DEGs through expression level and phylogenetic analyses. Positive regulators identified were *LjMYB112*, *MYB-related66*, *LjbHLH20*, and *LjbHLH23*, while negative regulators included *LjMYB49*, *LjMYB70*, *LjMYB107*, *LjMYB75*, *LjMYB111*, *LjMYB13*, *LjMYB54*, *MYB-related34*, *MYB-related36*, and *MYB-related42* (Figure 9). In kiwifruit, the AcMYBF110-AcbHLH1-AcWDR1 complex regulates anthocyanin biosynthesis by directly binding to the promoters of anthocyanin synthesis genes (Liu *et al.*, 2021), whereas AmMYB308 in *Antirrhinum majus*, AtMYBL2 in *Arabidopsis thaliana*, GtMYB1R1 and GtMYB1R9 in *Gentiana trifloral*, PhMYB27 and PhMYBx in *Petunia hybrida* have been reported as negative regulators in anthocyanin biosynthesis (Yan *et al.*, 2021). Similarly, *bHLH92 in Leymus chinensis (Zhao et al., 2019), CpbHLH1* in *Chimonanthus praecox* (Zhao *et al.*, 2020), and SmbHLH1 in Solanum melongena(Duan *et al.*, 2021) has been reported as repressors in the anthocyanin biosynthesis. Additionally, *bZIP39*, *ERF50*, *MADS-M-type28*, *MADS-MIKC9*, *NAC74*, *NAC81*, *NAC17*, *WRKY15*, *WRKY39*, and *WRKY49* were differentially expressed between LjR and LjW, suggesting that these TFs may also regulate or influence the structural and regulatory genes involved in anthocyanin production. These findings provide insights into the regulatory networks of anthocyanin biosynthesis in honeysuckle and offer a biological basis for developing new honeysuckle cultivars. The future research will be focused on the identification of candidate transcription factor functions.

Conclusions

Red honeysuckle is a valuable germplasm resource, yet little is known about its red pigment composition, anthocyanin biosynthesis pathway, and regulation mechanism. This study revealed that the major red pigment components in red honeysuckle were cyanidin-3,5-O-diglucoside (633.5 μg/g), peonidin-3,5-O-diglucoside (73.935 μg/g), and cyanidin-3-O-glucoside (3.75 μg/g). The high expression of *F3H1*, *F3'H*, *DFR1*, *ANS2*, *ANS3*, *UFGT4* and *UFGT8* genes in red honeysuckle probably accounted for its red coloration. Additionally, bHLH23 may regulate anthocyanins biosynthesis by binding to the *DFR1* gene promoter and promoting its expression. These findings can facilitate the cultivation of new honeysuckle varieties and the development of functional foods and medicines.

Authors' Contributions

Conceptualization, X.Z. and C.L.; Methodology, X.Z. and C.L.; Formal analysis, X.Z. and C.L.; Investigation, X.Z. and C.L.; Resources, Z.H.; Data curation, Z.X.; Writing–original draft preparation, X.Z. and C.L.; Writing–review and editing, X.Z. and C.L.; Funding acquisition, X.Z. and C.L. All authors read and approved the final manuscript.

Ethical approval (for researches involving animals or humans)

Not applicable.

Acknowledgements

This work was supported by the General Project of Henan Provincial Natural Science Foundation, grant number: 232300420027, the Excellent Research Support and Entrepreneurship Startup Project for Overseas Chinese Scholars at Department of Human Resources and Social Security of Henan Province, grant number: 2023039, and the Start-up Fee for Doctoral Scientific Research at Xuchang University, grant numbers: 20201009 and 20201010.

Conflict of Interests

The authors declare that there are no conflicts of interest related to this article.

References

Albert NW, Davies KM, Lewis DH, Zhang H, Montefiori M, Brendolise C, Boase MR, Ngo H, Jameson PE, Schwinn KE (2014). A conserved network of transcriptional activators and repressors regulates anthocyanin pigmentation in eudicots. Plant Cell 26(3):962-980. *https://doi.org/10.1105/tpc.113.122069*

An JP, Zhang XW, Bi SQ, You CX, Wang XF, Hao YJ (2020). The ERF transcription factor MdERF38 promotes drought stress-induced anthocyanin biosynthesis in apple. Plant Journal 101(3):573-589. *https://doi.org/10.1111/tpj.14555*

An JP, Zhang XW, You CX, Bi SQ, Wang XF, Hao YJ (2019). MdWRKY40 promotes wounding-induced anthocyanin biosynthesis in association with MdMYB1 and undergoes MdBT2-mediated degradation. New Phytologist 224(1):380-395. *https://doi.org/10.1111/nph.16008*

Araguirang GE, Richter AS (2022). Activation of anthocyanin biosynthesis in high light–what is the initial signal? New Phytologist 236(6):2037-2043. *https://doi.org/10.1111/nph.18488*

Ben-Simhon Z, Judeinstein S, Trainin T, Harel-Beja R, Bar-Ya'akov I, Borochov-Neori H, Holland D (2015). A "White" anthocyanin-less pomegranate (*Punica granatum* L.) caused by an insertion in the coding region of the *leucoanthocyanidin dioxygenase* (*LDOX*; *ANS*) gene. PloS One 10(11):e0142777. *https://doi.org/10.1371/journal.pone.0142777*

Cai Z, Wang C, Chen C, Zou L, Yin S, Liu S, Yuan J, Wu N, Liu X (2022). Comparative transcriptome analysis reveals variations of bioactive constituents in *Lonicera japonica* flowers under salt stress. Plant Physiology Biochemistry 173:87-96. *https://doi.org/10.1016/j.plaphy.2022.01.022*

Cao W, Chen J, Li L, Ren G, Duan X, Zhou Q, Zhang M, Gao D, Zhang S, Liu X (2022). Cookies fortified with *Lonicera japonica* Thunb. extracts: impact on phenolic acid content, antioxidant activity and physical properties. Molecules 27(15):5033. *https://doi.org/10.3390/molecules27155033*

Chen Z, Yu L, Liu W, Zhang J, Wang N, Chen X (2021). Research progress of fruit color development in apple (*Malus domestica* Borkh.). Plant Physiology Biochemistry 162:267-279. *https://doi.org/10.1016/j.plaphy.2021.02.033*

Cui D, Zhao S, Xu H, Allan AC, Zhang X, Fan L, Chen L, Su J, Shu Q, Li K (2021). The interaction of MYB, bHLH and WD40 transcription factors in red pear (*Pyrus pyrifolia*) peel. Plant Molecular Biology 106(4-5):407-417. *https://doi.org/10.1007/s11103-021-01160-w*

da Silva FL, Escribano-Bailón MT, Pérez Alonso JJ, Rivas-Gonzalo JC, Santos-Buelga C (2007). Anthocyanin pigments in strawberry. LWT - Food Science and Technology 40(2):374-382. *https://doi.org/10.1016/j.lwt.2005.09.018*

Duan Z, Tian S, Yang G, Wei M, Li J, Yang F (2021). The basic Helix-Loop-Helix transcription factor SmbHLH1 represses anthocyanin biosynthesis in eggplant. Frontiers in Plant Science 12:757936. *https://doi.org/10.3389/fpls.2021.757936*

Editorial Committee of Flora of China (1988). Flora of China [中国植物志]. Science Press, Beijing. Volume 72, pp 236. *http://www.iplant.cn/info/Lonicera%20japonica?t=z*

Ge L, Xie Q, Jiang Y, Xiao L, Wan H, Zhou B, Wu S, Tian J, Zeng X (2022). Genus Lonicera: New drug discovery from traditional usage to modern chemical and pharmacological research. Phytomedicine 96:153889. *https://doi.org/10.1016/j.phymed.2021.153889*

Han MH, Lee WS, Nagappan A, Hong SH, Jung JH, Park C, Kim HJ, Kim GY, Kim G, Jung JM (2016). Flavonoids isolated from flowers of *Lonicera japonica* Thunb. inhibit inflammatory responses in BV2 microglial cells by suppressing TNF-α and IL-β through PI3K/Akt/NF-kb signaling pathways. Phytotherapy Research 30(11):1824-1832. *https://doi.org/10.1002/ptr.5688*

Han Y, Vimolmangkang S, Soria-Guerra RE, Rosales-Mendoza S, Zheng D, Lygin AV, Korban SS (2010). Ectopic expression of apple *F3'H* genes contributes to anthocyanin accumulation in the Arabidopsis *tt7* mutant grown under nitrogen stress. Plant Physiology 153(2):806-820. *https://doi.org/10.1104/pp.109.152801*

Johnson ET, Ryu S, Yi H, Shin B, Cheong H, Choi G (2001). Alteration of a single amino acid changes the substrate specificity of dihydroflavonol 4-reductase. Plant Journal 25(3):325-333. *https://doi.org/10.1046/j.1365-313x.2001.00962.x*

Khan IA, Cao K, Guo J, Li Y, Wang Q, Yang X, Wu J, Fang W, Wang L (2022). Identification of key gene networks controlling anthocyanin biosynthesis in peach flower. Plant Science 316:111151. *https://doi.org/10.1016/j.plantsci.2021.111151*

Kou Y, Li Z, Yang T, Shen X, Wang X, Li H, Zhou K, Li L, Xia Z, Zheng X, Zhao Y (2022). Therapeutic potential of plant iridoids in depression: a review. Pharmaceutical Biology 60(1):2167-2181. *https://doi.org/10.1080/13880209.2022.2136206*

LaFountain AM, Yuan YW (2021). Repressors of anthocyanin biosynthesis. New Phytologist 231(3):933-949.

Li J, Lian X, Ye C, Wang L (2019). Analysis of flower color variations at different developmental stages in two honeysuckle (*Lonicera Japonica* Thunb.) cultivars. HortScience 54(5):779-782. *https://doi.org/10.21273/HORTSCI13819-18*

Li J, Ma N, An Y, Wang L (2021). FcMADS9 of fig regulates anthocyanin biosynthesis. Scientia Horticulturae 278:109820. *https://doi.org/10.1016/j.scienta.2020.109820*

Li J, Yu X, Shan Q, Shi Z, Li J, Zhao X, Chang C, Yu J (2022). Integrated volatile metabolomic and transcriptomic analysis provides insights into the regulation of floral scents between two contrasting varieties of *Lonicera japonica*. Frontiers in Plant Science 13:989036. *https://doi.org/10.3389/fpls.2022.989036*

Liu M, Ma Z, Zheng T, Sun W, Zhang Y, Jin W, Zhan J, Cai Y, Tang Y, Wu Q, Tang Z, Bu T, Li C, Chen H (2018). Insights into the correlation between physiological changes in and seed development of tartary buckwheat (*Fagopyrum tataricum* Gaertn.). BMC Genomics 19(1):648. *https://doi.org/10.1186/s12864-018-5036-8*

Liu W, Mei Z, Yu L, Gu T, Li Z, Zou Q, Zhang S, Fang H, Wang Y, Zhang Z, Chen X, Wang N (2023). The ABA-induced NAC transcription factor MdNAC1 interacts with a bZIP-type transcription factor to promote anthocyanin synthesis in red-fleshed apples. Horticulture Research. *https://doi.org/10.1093/hr/uhad049*

Liu Y, Ma K, Qi Y, Lv G, Ren X, Liu Z, Ma F (2021). Transcriptional regulation of anthocyanin synthesis by MYB-bHLH-WDR complexes in kiwifruit (*Actinidia chinensis*). Journal of Agricultural and Food Chemistry 69(12):3677-3691. *https://doi.org/10.1021/acs.jafc.0c07037*

Lloyd A, Brockman A, Aguirre L, Campbell A, Bean A, Cantero A, Gonzalez A (2017). Advances in the MYB-bHLH-WD repeat (MBW) pigment regulatory model: addition of a WRKY factor and co-option of an anthocyanin MYB for betalain regulation. Plant & Cell Physiology 58(9):1431-1441. *https://doi.org/10.1093/pcp/pcx075*

Lu Z, Cao H, Pan L, Niu L, Wei B, Cui G, Wang L, Yao JL, Zeng W, Wang Z (2021). Two loss-of-function alleles of the *glutathione S-transferase* (*GST*) gene cause anthocyanin deficiency in flower and fruit skin of peach (*Prunus persica*). Plant Journal 107(5):1320-1331. *https://doi.org/10.1111/tpj.15312*

Mao X, Cai T, Olyarchuk JG, Wei L (2005). Automated genome annotation and pathway identification using the KEGG Orthology (KO) as a controlled vocabulary. Bioinformatics 21(19):3787-3793. *https://doi.org/10.1093/bioinformatics/bti430*

Muhammad N, Luo Z, Yang M, Li X, Liu Z, Liu M (2022). The joint role of the late anthocyanin biosynthetic UFGT-encoding genes in the flowers and fruits coloration of horticultural plants. Scientia Horticulturae 301:111110. *https://doi.org/10.1016/j.scienta.2022.111110*

National Pharmacopoeia Committee (2020). Chinese Pharmacopoeia [中国药典]. China Medical Science and Technology Press, Beijing. Volume 1, pp 201+230-232. *https://db.ouryao.com/yd2020/view.php?id=f5ed4097cc*; *https://db.ouryao.com/yd2020/view.php?id=f5cde5c826*

Ni J, Bai S, Zhao Y, Qian M, Tao R, Yin L, Gao L, Teng Y (2019). Ethylene response factors Pp4ERF24 and Pp12ERF96 regulate blue light-induced anthocyanin biosynthesis in 'Red Zaosu' pear fruits by interacting with MYB114. Plant Molecular Biology 99(1-2):67-78. *https://doi.org/10.1007/s11103-018-0802-1*

Oboh G, Agunloye OM, Akinyemi AJ, Ademiluyi AO, Adefegha SA (2013). Comparative study on the inhibitory effect of caffeic and chlorogenic acids on key enzymes linked to Alzheimer's disease and some pro-oxidant induced oxidative stress in rats' brain-*in vitro*. Neurochemical Research 38:413-419. *https://doi.org/10.1007/s11064-012-0935-6*

Pertea M, Pertea GM, Antonescu CM, Chang TC, Mendell JT, Salzberg SL (2015). StringTie enables improved reconstruction of a transcriptome from RNA-seq reads. Nature Biotechnology 33(3):290-295. *https://doi.org/10.1038/nbt.3122*

Petit P, Granier T, d'Estaintot BL, Manigand C, Bathany K, Schmitter JM, Lauvergeat V, Hamdi S, Gallois B (2007). Crystal structure of grape dihydroflavonol 4-reductase, a key enzyme in flavonoid biosynthesis. Journal of Molecular Biology 368(5):1345-1357. *https://doi.org/10.1016/j.jmb.2007.02.088*

Pu X, Li Z, Tian Y, Gao R, Hao L, Hu Y, He C, Sun W, Xu M, Peters RJ, Van de Peer Y, Xu Z, Song J (2020). The honeysuckle genome provides insight into the molecular mechanism of carotenoid metabolism underlying dynamic flower coloration. New Phytologist 227(3):930-943. *https://doi.org/10.1111/nph.16552*

Qi F, Liu Y, Luo Y, Cui Y, Lu C, Li H, Huang H, Dai S (2022). Functional analysis of the ScAG and ScAGL11 MADS-box transcription factors for anthocyanin biosynthesis and bicolour pattern formation in *Senecio cruentus* ray florets. Horticulture Research 9:uhac071. *https://doi.org/10.1093/hr/uhac071*

Reis JF, Monteiro VV, de Souza Gomes R, do Carmo MM, da Costa GV, Ribera PC, Monteiro MC (2016). Action mechanism and cardiovascular effect of anthocyanins: a systematic review of animal and human studies. Journal of Translational Medicine 14(1):315. *https://doi.org/10.1186/s12967-016-1076-5*

Shang X, Pan H, Li M, Miao X, Ding H (2011). *Lonicera japonica* Thunb.: ethnopharmacology, phytochemistry and pharmacology of an important traditional Chinese medicine. Journal of Ethnopharmacology 138(1):1-21. *https://doi.org/10.1016/j.jep.2011.08.016*

Shannon P, Markiel A, Ozier O, Baliga NS, Wang JT, Ramage D, Amin N, Schwikowski B, Ideker T (2003). Cytoscape: a software environment for integrated models of biomolecular interaction networks. Genome Research 13(11):2498-2504. *https://doi.org/10.1101/gr.1239303*

Sun Q, Jiang S, Zhang T, Xu H, Fang H, Zhang J, Su M, Wang Y, Zhang Z, Wang N, Chen X (2019). Apple NAC transcription factor MdNAC52 regulates biosynthesis of anthocyanin and proanthocyanidin through MdMYB9 and MdMYB11. Plant Science 289:110286. *https://doi.org/10.1016/j.plantsci.2019.110286*

Wang H, Fan W, Li H, Yang J, Huang J, Zhang P (2013). Functional characterization of dihydroflavonol-4-reductase in anthocyanin biosynthesis of purple sweet potato underlies the direct evidence of anthocyanins function against abiotic stresses. PloS One 8(11):e78484. *https://doi.org/10.1371/journal.pone.0078484*

Wang H, Li Y, Wang S, Kong D, Sahu SK, Bai M, Li H, Li L, Xu Y, Liang H (2020). Comparative transcriptomic analyses of chlorogenic acid and luteolosides biosynthesis pathways at different flowering stages of diploid and tetraploid *Lonicera japonica*. PeerJ 8:e8690. *https://doi.org/10.7717/peerj.8690*

Wang S, Zhang X, Li B, Zhao X, Shen Y, Yuan Z (2022). Genome-wide identification and characterization of bZIP gene family and cloning of candidate genes for anthocyanin biosynthesis in pomegranate (*Punica granatum*). BMC Plant Biology 22(1):170. *https://doi.org/10.1186/s12870-022-03560-6*

Wang X, Chen X, Luo S, Ma W, Li N, Zhang W, Tikunov Y, Xuan S, Zhao J, Wang Y, Zheng G, Yu P, Bai Y, Bovy A, Shen S (2022). Discovery of a *DFR* gene that controls anthocyanin accumulation in the spiny Solanum group: roles of a natural promoter variant and alternative splicing. Plant Journal 111(4):1096-1109. *https://doi.org/10.1111/tpj.15877*

Wang Y, Li L, Ji W, Liu S, Fan J, Lu H, Wang X (2023) Metabolomics analysis of different tissues of *Lonicera japonica* Thunb. based on liquid chromatography with mass spectrometry. Metabolites 13(2):186 *https://doi.org/10.3390/metabo13020186*

Wu T, Hu E, Xu S, Chen M, Guo P, Dai Z, Feng T, Zhou L, Tang W, Zhan L, Fu X, Liu S, Bo X, Yu G (2021). clusterProfiler 4.0: A universal enrichment tool for interpreting omics data. Innovation (Camb) 2(3):100141. *https://doi.org/10.1016/j.xinn.2021.100141*

Wu X, Gong Q, Ni X, Zhou Y, Gao Z (2017). UFGT: the key enzyme associated with the petals variegation in Japanese apricot. Frontiers in Plant Science 8:108. *https://doi.org/10.3389/fpls.2017.00108*

Wu Y, Zhang C, Huang Z, Lyu L, Li W, Wu W (2022). Integrative analysis of the metabolome and transcriptome provides insights into the mechanisms of flavonoid biosynthesis in blackberry. Food Research International 153:110948. *https://doi.org/10.1016/j.foodres.2022.110948*

Xia Y, Chen W, Xiang W, Wang D, Xue B, Liu X, Xing L, Wu D, Wang S, Guo Q, Liang G (2021). Integrated metabolic profiling and transcriptome analysis of pigment accumulation in *Lonicera japonica* flower petals during colour-transition. BMC Plant Biology 21(1):98. *https://doi.org/10.1186/s12870-021-02877-y*

Xiao Q, Li Z, Qu M, Xu W, Su Z, Yang J (2021). LjaFGD: *Lonicera japonica* functional genomics database. Journal of Integrative Plant Biology 63(8):1422-1436. *https://doi.org/10.1111/jipb.13112*

Xu Y, Zhao G, Ji X, Liu J, Zhao T, Gao Y, Gao S, Hao Y, Gao Y, Wang L, Weng X, Chen Z, Jia L (2022). Metabolome and transcriptome analysis reveals the transcriptional regulatory mechanism of triterpenoid saponin biosynthesis in soapberry (*Sapindus mukorossi* Gaertn.). Journal of Agricultural and Food Chemistry 70(23):7095-7109. *https://doi.org/10.1021/acs.jafc.2c01672*

Yan H, Pei X, Zhang H, Li X, Zhang X, Zhao M, Chiang VL, Sederoff RR, Zhao X (2021). MYB-mediated regulation of anthocyanin biosynthesis. International Journal of Molecular Sciences 22(6):3103. *https://doi.org/10.3390/ijms22063103*

Yang B, Zhong Z, Wang T, Ou Y, Tian J, Komatsu S, Zhang L (2019). Integrative omics of *Lonicera japonica* Thunb. Flower development unravels molecular changes regulating secondary metabolites. Journal of Proteomics 208:103470. *https://doi.org/10.1016/j.jprot.2019.103470*

Yi D, Zhang H, Lai B, Liu L, Pan X, Ma Z, Wang Y, Xie J, Shi S, Wei Y (2021). Integrative analysis of the coloring mechanism of red longan pericarp through metabolome and transcriptome analyses. Journal of Agricultural and Food Chemistry 69(6):1806-1815. *https://doi.org/10.1021/acs.jafc.0c05023*

Young MD, Wakefield MJ, Smyth GK, Oshlack A (2010). Gene ontology analysis for RNA-seq: accounting for selection bias. Genome Biology 11(2):R14. *https://doi.org/10.1186/gb-2010-11-2-r14*

Yu H, Cui N, Guo K, Xu W, Wang H (2022). Epigenetic changes in the regulation of carotenoid metabolism during honeysuckle flower development. Horticultural Plant Journal. *https://doi.org/10.1016/j.hpj.2022.11.003*

Yuan Y, Song L, Li M, Liu G, Chu Y, Ma L, Zhou Y, Wang X, Gao W, Qin S, Yu J, Wang X, Huang L (2012). Genetic variation and metabolic pathway intricacy govern the active compound content and quality of the Chinese medicinal plant *Lonicera japonica* thunb. BMC Genomics 13(1):195. *https://doi.org/10.1186/1471-2164-13-195*

Zhang L, Hou D, Chen X, Li D, Zhu L, Zhang Y, ... Zhang CY (2012). Exogenous plant MIR168a specifically targets mammalian LDLRAP1: evidence of cross-kingdom regulation by microRNA. Cell Research 22(1):107-126. *https://doi.org/10.1038/cr.2011.158*

Zhang S, Chen Y, Zhao L, Li C, Yu J, Li T, Yang W, Zhang S, Su H, Wang L (2020). A novel NAC transcription factor, MdNAC42, regulates anthocyanin accumulation in red-fleshed apple by interacting with MdMYB10. Tree Physiology 40(3):413-423. *https://doi.org/10.1093/treephys/tpaa004*

Zhang X, Allan A, Chen X, Fan L, Chen L, Shu Q, Su J, Li K (2012). Coloration, anthocyanin profile and metal element content of Yunnan Red Pear (*Pyrus pyrifolia*). Horticultural Science 39(4):164-171. *https://doi.org/10.17221/265/2011-HORTSCI*

Zhang Y, Cheng Y, Xu S, Ma H, Han J, Zhang Y (2020). Tree peony variegated flowers show a small insertion in the F3'H gene of the acyanic flower parts. BMC Plant Biology 20(1):211. *https://doi.org/10.1186/s12870-020-02428-x*

Zhao D, Tao J (2015). Recent advances on the development and regulation of flower color in ornamental plants. Frontiers in Plant Science 6: 261. *https://doi.org/10.3389/fpls.2015.00261*

Zhao P, Li X, Jia J, Yuan G, Chen S, Qi D, Cheng L, Liu G (2019). bHLH92 from sheepgrass acts as a negative regulator of anthocyanin/proanthocyandin accumulation and influences seed dormancy. Journal of Experimental Botany 70(1):269-284. *https://doi.org/10.1093/jxb/ery335*

Zhao R, Song X, Yang N, Chen L, Xiang L, Liu XQ, Zhao K (2020). Expression of the subgroup IIIf bHLH transcription factor CpbHLH1 from *Chimonanthus praecox* (L.) in transgenic model plants inhibits anthocyanin accumulation. Plant Cell Reports 39(7):891-907. *https://doi.org/10.1007/s00299-020-02537-9*

Zhao ZC, Hu GB, Hu FC, Wang HC, Yang ZY, Lai B (2012). The UDP glucose: flavonoid-3-O-glucosyltransferase (UFGT) gene regulates anthocyanin biosynthesis in litchi (*Litchi chinesis* Sonn.) during fruit coloration. Molecular Biology Reports 39(6):6409-6415. *https://doi.org/10.1007/s11033-011-1303-3*

Zheng Y, Jiao C, Sun H, Rosli Hernan G, Pombo Marina A, Zhang P, ... Fei Z (2016). iTAK: A Program for genome-wide prediction and classification of plant transcription factors, transcriptional regulators, and protein kinases. Molecular Plant 9(12):1667-1670. *https://doi.org/10.1016/j.molp.2016.09.014*

Zhou H, Wang LK, Wang H, Gu C, Dare AP, Espley RV, He H, Allan AC, Han Y (2015). Molecular genetics of blood-fleshed peach reveals activation of anthocyanin biosynthesis by NAC transcription factors. Plant Journal 82(1):105-121. *https://doi.org/10.1111/tpj.12792*

Zhou Z, Li X, Liu J, Dong L, Chen Q, Liu J, ... Zhang CY (2015). Honeysuckle-encoded atypical microRNA2911 directly targets influenza A viruses. Cell Research 25(1):39-49. *https://doi.org/10.1038/cr.2014.130*

- Maps and affiliations: The publisher stay neutral with regard to jurisdictional claims in published maps and institutional affiliations.
- Responsibilities: The editors, editorial board and publisher do not assume any responsibility for the article's contents and for the authors' views expressed in their contributions. The statements and opinions published represent the views of the authors or persons to whom they are credited. Publication of research information does not constitute a recommendation or endorsement of products involved.